ORIGINAL RESEARCH

Green one-pot preparation of carbon dots (CD)-embedded cellulose transparent film for Fe^{3+} indicator using ionic liquid

Jeongyeon Woo · Younghan Song · Jungbin Ahn · Hyungsup Kim

Abstract In this study, carbon dots (CD)-embedded film was successfully fabricated for Fe^{3+} sensing via a one-pot process. The carbon dots for Fe^{3+} ion detection were synthesized using the cellulose/ionic liquid solution for different treatment times. With the increase of the treatment time, the N-doped graphitic structure in the core and the functional groups on the surface were highly developed in the carbon dots. The properties and structures of the carbon dots were characterized using TEM, UV–Vis spectroscopy, XPS, IR, TCSPC, and PL spectroscopy. The carbon dots prepared by 12 h treatment showed a high quantum yield of 28.4%, and the superior stability for long-term storage, UV exposure, ionic strength, and pH change. The carbon dots in the film, as well as in the aqueous dispersion, revealed highly selective detection toward Fe^{3+}. The CD-embedded cellulose film can be used as a Fe^{3+} indicating film with good reusability, outstanding transparency, and high photostability.
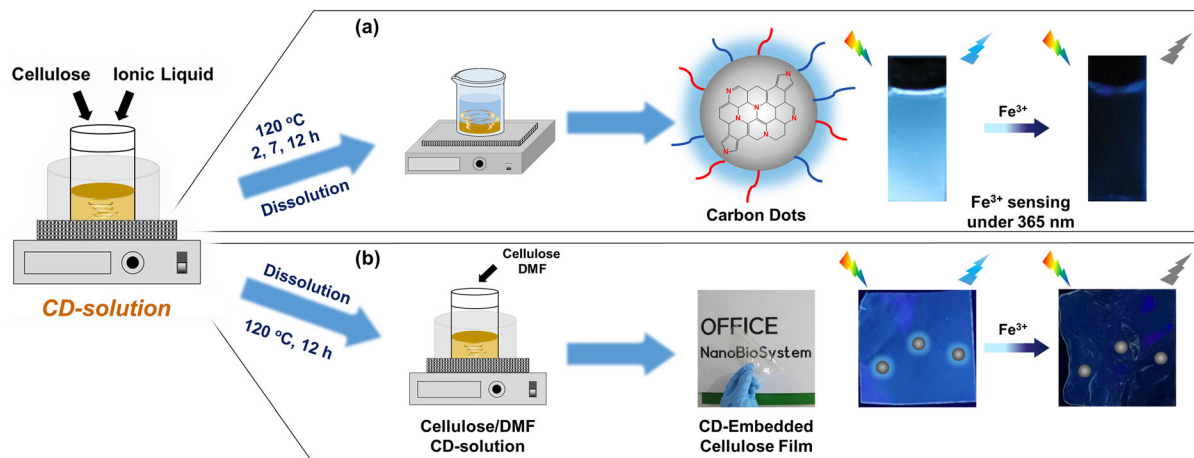

Jeongyeon Woo and Younghan Song have contributed equally to this work.

J. Woo · Y. Song · J. Ahn · H. Kim (✉)
Department of Organic and Nano System Engineering, Konkuk University, Seoul 05029, Republic of Korea
e-mail: iconclast@konkuk.ac.kr

H. Kim
Division of Chemical Engineering, Konkuk University, Seoul 05029, Republic of Korea

Graphic abstract

Introduction

Recently, carbon dots have been received increasing attention for one of the zero-dimensional nanomaterials. Ranging in size from 1 to 10 nm, the carbon dots are generally composed of carbon core with sp^2 hybridized networks and surface with various functional groups (da Silva Souza et al. 2018). They have great potentials for a wide range of applications because of their chemical, morphological and structural merits such as good biocompatibility, nano-size (< 10 nm), water-solubility, chemical inertness, stable photoluminescence (PL), etc. (Ahn et al. 2019; Guo et al. 2016; Yang et al. 2014). Since the first discovery of carbon dots, different types of synthesizing methods were reported including hydrothermal, solvothermal, electrochemical and microwave-assisted syntheses (Guo et al. 2016; He et al. 2017; Loi et al. 2017; Lu et al. 2009). Among those processes, hydrothermal synthesis (HTS) has been extensively studied to apply various polymeric precursors for the fabrication of carbon dots. For sustainable developments, biomasses were used as the precursors of carbon dots for high performance and functionality (Ahn et al. 2019; Gu et al. 2016; Yang et al. 2014). Among the biomasses, cellulose is an attractive precursor for carbon dots due to many

beneficial properties, such as low price, eco-friendly, non-toxic, good biocompatibility and stable chemical properties. In addition, it is the most abundant polymer on earth and produced more than 100 billion tons per year (Trache et al. 2017). By HTS of cellulose, several types of carbogenic materials including carbon dots can be fabricated in a top-down manner. Sevilla and Fuertes (2009) suggested the carbonization mechanism of cellulose by HTS as the following two steps. First, in temperature higher than 220 °C, cellulose is hydrolyzed, decomposed or dehydrated to water-soluble molecules such as oligomers, aldehydes, phenols, acids, etc. Second, these soluble products are condensed and aromatized to grow carbogenic materials. Although the HTS can effectively synthesize carbon dots, it requires a special vessel that can withstand the self-generated pressure or the acidic condition during the process. Also, the processing temperature of HTS needs to be higher than 200 °C for the carbonization of cellulose, consuming a large amount of heat energy (Wu et al. 2017; Yang et al. 2016). After hydrothermal synthesis, the additional separation from the micro-sized products of the HTS was unavoidable to obtain carbon dots. The micro-sized particles such as amorphous carbon particles and debris of cellulose can be filtered using chromatography, dialysis or centrifuge (Song et al. 2017). In order to fabricate carbon dots in an economic and efficient way, several solution processes using green solvents were reported (Gu et al. 2018; Wang et al. 2016). Among those green solvents, ionic liquids (ILs) take a large amount of attention in many areas. ILs are

charming "green solvent systems" with promising properties, including negligible vapor pressure, high thermal stabilities, high polarity and good recyclability (Huddleston et al. 2001; Wang et al. 2014; Wei et al. 2012). ILs are reliable solvents of various biomass-based polymers such as cellulose, chitin, and starch (Silva et al. 2017; Wu et al. 2009; Zhang et al. 2014). As well known, some ILs can hydrolyze cellulose chains into water-soluble molecules during dissolution and incubation (Ahn et al. 2016a, b, 2017b; Du and Qian 2011; Kim et al. 2016; Lee et al. 2009). This can give an opportunity to synthesize carbon dots via solution carbonization of cellulose under proper depolymerizations and precipitation. Although a few researchers have reported on the usage of IL for carbon dots fabrication, the depolymerization of IL was not applied for carbon dots fabrication. Liu et al. (2015) used IL (1-ally-3-methylimidazolium chloride) as nitrogen source when they fabricated carbon dots via hydrothermal synthesis from rice straw. Wang et al. (2016) used IL (1-butyl-3-methylimidazolium chloride) as solvent and catalyst for carbon dots fabrication at low temperature (80 °C). The carbon dots showed Hg^{2+} detecting capability and good photoluminescence stability. However, the quantum yield (QY) of the carbon dots was too low as 4.7% for further applications. Still, the solution process for carbon dots from cellulose has not been fully exploited.

In this work, we suggest a simple method for fabricating carbon dots using 1-butyl-3-methylimidazolium acetate (BMIMOAc) via solution synthesis of cellulose. The QYs of the prepared carbon dots were dramatically increased from 4 to 28.4% by increasing the treatment time from 2 to 12 h. The carbon dots showed high selectivity and sensitivity toward Fe^{3+}. Furthermore, a carbon dots (CD)-embedded cellulose transparent film was prepared via a one-pot process without extra separation of the carbon dots. The CD-embedded film also showed a good detecting capability of Fe^{3+} as an indicating film. To the best of our knowledge, it is the first report on the one-pot fabrication process for a fluorescent and transparent film from cellulose via solution process.
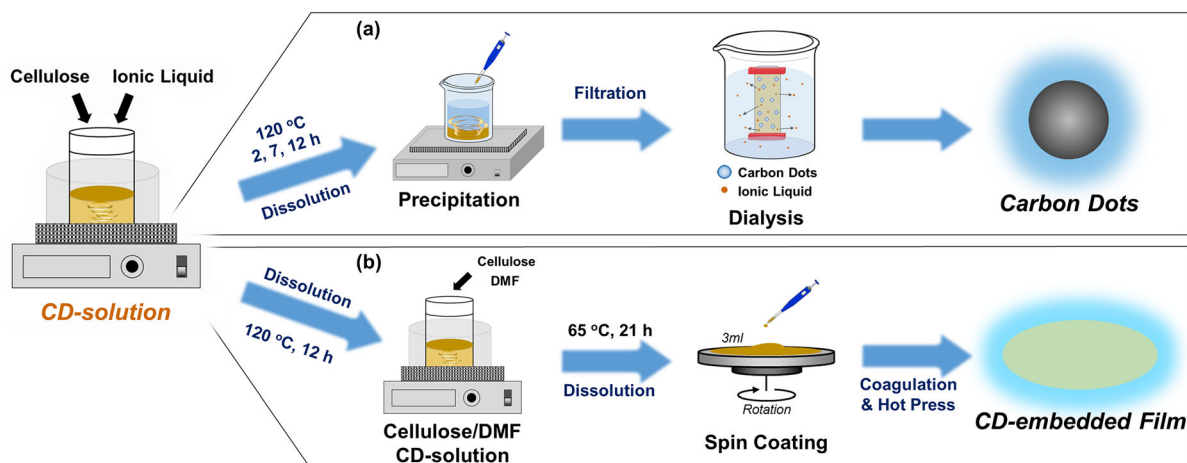
Experimental

Materials

Two types of cellulose were used for the fabrication of carbon dots and CD-embedded film. One is MCC (microcrystalline cellulose, degree of polymerization: 200, Sigma Aldrich) for carbon dots and the other is kraft pulp (degree of polymerization: 1100, Hyosung Co.) for the film. 1-butyl-3-methylimidazolium acetate (BMIMOAc, > 95%, Sigma Aldrich) was used for cellulose dissolution. All metal salts for metal ion detection were purchased from Sigma Aldrich. The materials in the study were used as received without purification.

Synthesis of the carbon dots

The carbon dots were prepared as illustrated in Scheme 1a. 7 wt% of MCC was dissolved in BMIMOAc at 120 °C for 2, 7 and 12 h, respectively. After the designated dissolution time, the solution was poured in distilled water for precipitation. The precipitated solutions including the carbon dots were gently stirred until the ionic liquid (IL) was completely removed. The solution was filtrated to obtain the carbon dots using a nylon membrane of 0.45 μm pore and the filtrate was completely dried. For further purification of the carbon dots, the dried filtrate was dispersed in ethanol and then dialyzed against ethanol for 120 h to remove the residual IL. The obtained carbon dots were named after the dissolution time. For example, CD-2 refers to the carbon dots produced after 2 h dissolution by IL.

One-pot fabrication of CDs-embedded film

The CD-embedded film was directly fabricated by the dissolution of kraft pulp in the prepared CD-solution as follows (see Scheme 1b): First, CD-solution was prepared by dissolution of MCC in BMIMOAc with the concentration 7 wt% for 12 h at 120 °C. After adding *N, N*-dimethylformamide (DMF, > 99.5%, Daejung Co., 1:1 (w/w) with respect to IL) to the solution, kraft pulp was added and dissolved in the CD-solution without precipitation of the carbon dots. Using the prepared solution, the film was cast according to the previous report (Kim et al. 2018). Briefly, the prepared solution was spin-coated on a

Scheme 1 Experimental procedure: **a** Synthesis of carbon dots using cellulose/ionic liquid solution. **b** one-pot fabrication method of CD-embedded film

glass substrate at 1500 rpm. Before the as-cast film was coagulated, the film was kept on the substrate for 30 min in an oven at 70 °C for stress relaxation. After the treatment, the film was immersed in distilled water to remove the solvents. After washing 5 times by distilled water, the solidified film was pressed and dried at 135 °C for 35 min using a hot-pressing machine. The CD-embedded film was named CD-F.

Characterizations

High-resolution transmission electron microscopy (TEM, JEM-F200, JEOL) was applied to study morphology. The FFT (fast Fourier transform) spot diagrams of the prepared carbon dots were obtained under the operating voltage of 200 kV. The functional groups and the binding species were characterized using Fourier-transform infrared spectroscopy (FT-IR, Nicolet iS10, Thermo Scientific) and X-ray photoelectron spectroscopy (XPS, K-alpha, Thermo Scientific). The photoluminescence (PL) properties of the samples were studied using UV–Vis absorption spectroscopy (Cary 60 UV/vis spectrophotometer, Agilent Technologies) and PL spectroscopy (FS-2, SICNCO). The absolute fluorescence quantum yield (QY) of carbon dots was characterized at the excitation wavelength of 340 nm using PL spectroscopy equipped with the integrating sphere. The QY of the carbon dots were calculated according to Eq. (1).

$$QY(\Phi) = \frac{N_{emission}}{N_{absorption}} = \frac{\int \frac{\lambda}{hc} \left\{ I_{em}^{sam}(\lambda) - I_{em}^{ref}(\lambda) \right\} d\lambda}{\int \frac{\lambda}{hc} \left\{ I_{ex}^{ref}(\lambda) - I_{ex}^{sam}(\lambda) \right\} d\lambda}$$

(1)

where $N_{absorption}$ is the number of photons absorbed by a sample and $N_{emission}$ is the number of photons emitted from a sample. h, c, λ refer to the Planck's constant, velocity of light and wavelength, respectively. I_{ex}^{sam} and I_{ex}^{ref} are the integrated intensities of the excitation light with and without a sample, and I_{em}^{sam} and I_{em}^{ref} refers to the photoluminescence (PL) intensities with and without a sample, respectively (Ishida et al. 2010).

Metal ion sensing evaluation

For the detecting test of metal ions, $FeCl_3 \cdot 6H_2O$, $ZnCl_2$, $CuCl_2 \cdot H_2O$, $AgNO_3$, $FeCl_2 \cdot 4H_2O$, $CaCl_2$, $HgCl_2$, $AlCl_3 \cdot 6H_2O$, $Pb(NO_3)_2$ and $MgCl_2 \cdot 6H_2O$ were dissolved in distilled water with a concentration of 250 μM. The prepared CD-12 solution of 50 μg/ml was added to each metal ion solutions with 1:1 (v/v). After 15 min of mixing, the PL intensities of CD-12 in each metal ion solution were measured at 340 nm of excitation wavelength. For the sensitivity test of CD-12 for Fe^{3+} sensing, the PL intensities of the quenched CD-12 were characterized along with the concentration of Fe^{3+} solution using an excitation wavelength of 340 nm. For an indicator of Fe^{3+}, the prepared films (2 × 2 cm) were dipped in the Fe^{3+} solutions for 30 s. The PL intensities of the films were measured at

360 nm of excitation wavelength after dried at room temperature. For the cycling test, the quenched films were washed using 500 ml of distilled water for 30 min and the recovered films were dipped in 500 μM of Fe^{3+} again. Then the PL intensities of the films were measured at the same excitation wavelength after dried at RT. The cycling test was repeated 3 times.

pH stability of the carbon dots

For the test of pH stability, the photoluminescence behavior of CD-12 was characterized in the pH range from 1 to 13 using hydrochloric acid (HCl, 35–57%, Duksan Co.) and sodium hydroxide (NaOH, 98%, Daejung Co.). CD-12 was added and dispersed as a concentration of 50 μg/ml in each pH aqueous solution.

Results and discussion

Figure 1 shows the morphologies of the carbon dots prepared from MCC/BMIMOAc solution for different treatment times. The carbon dots had pseudo-spherical shapes with a graphitic lattice structure. It indicates that the carbon dots were successfully fabricated in the ionic liquid (IL). As reported in the previous work (Ahn et al. 2016a, b, 2017b; Du and Qian 2011; Kim et al. 2016; Lee et al. 2009), cellulose can be depolymerized via acid-catalyzed hydrolysis into small molecules in IL. In this hydrolysis, IL kept changing into carbene, which generates acid continuously. During those processes, the carbon dots were formed by the polymerization, condensation, and aromatization of the water-soluble small molecules such as oligomers, aldehydes, phenols, acids, etc. (Wang et al. 2016; Yang et al. 2017). The average size and its deviation of the carbon dots were increased with the treatment time. It can be attributed to homogenous nucleation and growth. As well explained in the thermodynamics of nanoparticle, the nucleus was generated in super-saturated conditions to reduce the total volume energy of the solution system. The size and variation of the resulted particles were dependent on how fast and long the nucleation occurs. If the nucleus was generated fast in a short time, the size and its variation of the resulted nanoparticles would be small. In this study, the nucleation time was

short, resulting in small and uniform carbon dots when the treatment times were 2 and 7 h. However, the size and its variation of the carbon dots became significantly larger when the treatment was 12 h, mainly due to the longer nucleation and growth time. After the nucleation, the nucleus growth is controlled by surface-reaction and diffusion of the composing molecules (He et al. 2017; Ng et al. 2017; Xu et al. 2013; Yang et al. 2017; Zheng et al. 2015).

The crystal lattice became distinct with the increase of the treatment time because the core had enough time to be developed into the graphitic structure. When the treatment time was 2 h, the low crystalline structure was observed. The carbon dots from 7 h treatment showed clear lattice fringe corresponding to the in-plane lattice spacing of the (100) graphene facet (0.21 nm) (Nie et al. 2014). Similarly, the lattice fringe corresponding to the in-plane lattice spacing of the (020) graphene facet (0.26 nm) was distinctly observed for the carbon dots from 12 h treatment (Nie et al. 2014). The acid generated by IL condensed and developed the carbogenic structure to the ordered graphitic structure in the core of the carbon dots (Ahn et al. 2016b; Börjesson and Westman 2015; MináKim et al. 2015).

The FT–IR spectra of the prepared carbon dots, MCC and BMIMOAc were displayed in Fig. 2a. The chemical structures of the prepared carbon dots were different from MCC and BMIMOAc. The MCC had typical characteristic peaks of cellulose at 3325, 2900, 1430–1316 and 1025 cm^{-1} corresponding to $\nu(O–H)$, $\nu(C–H)$, $\delta(C–H)$ and $\nu(C–O–C)$ respectively (Abderrahim et al. 2015; Ou et al. 2012). Also, the characteristic peaks of BMIMOAc were shown as fingerprint regions of the imidazolium ring from 1500 to 750 cm^{-1} and $\nu(O–C–O)$ at 1575 cm^{-1} and 1378 cm^{-1} (Tan et al. 2016; Yesudass et al. 2016; Zhang et al. 2015). Whereas, the carbon dots in the study had the similar infrared absorption pattern in $\nu(N–H)$, $\nu(O–H)$ band around 3440 cm^{-1}, $\nu(C=O)$ at 1654 cm^{-1}, aromatic C–N heterocyclic rings at 1400–1430 cm^{-1}, $\nu(C–N)$ at 1226 cm^{-1}, $\nu(C–O–C)$ at 1050 cm^{-1} and $\nu(N–H)$ at 800 cm^{-1} (Arul et al. 2017; Coates 2000; Liu and Zhou 2017; Liu et al. 2011; Ren et al. 2019; Su et al. 2019; Wu et al. 2017; Xiao et al. 2016). It demonstrates that all carbon dots had graphitic domains ($\nu(C=C)$ at 1654 cm^{-1}) with functional groups such as amino, carboxyl, carbonyl, and hydroxyl groups (Arul et al. 2017; Chae et al.
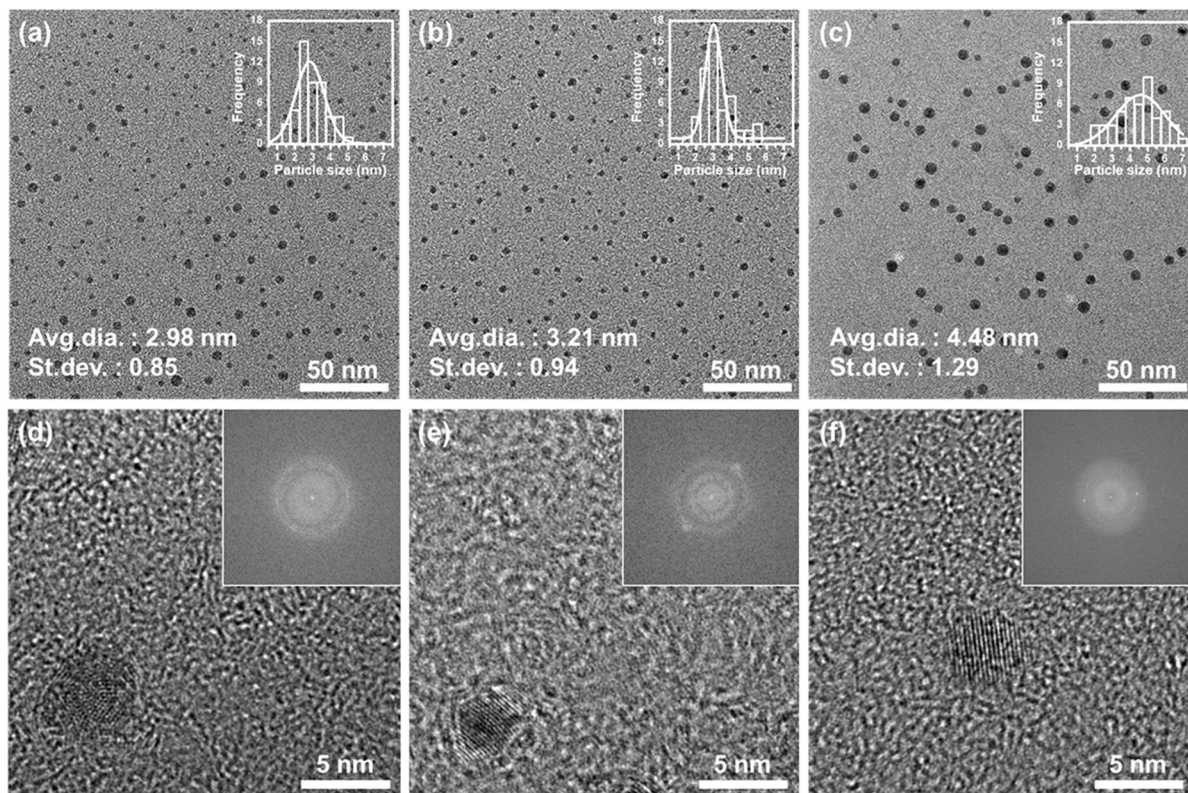
Fig. 1 TEM images of **a** CD-2, **b** CD-7, and **c** CD-12. HR-TEM images of **d** CD-2, **e** CD-7 and **f** CD-12 (inserted images in TEM and HR-TEM are size distribution and fast Fourier transform (FFT) spot diagrams of the carbon dots), respectively
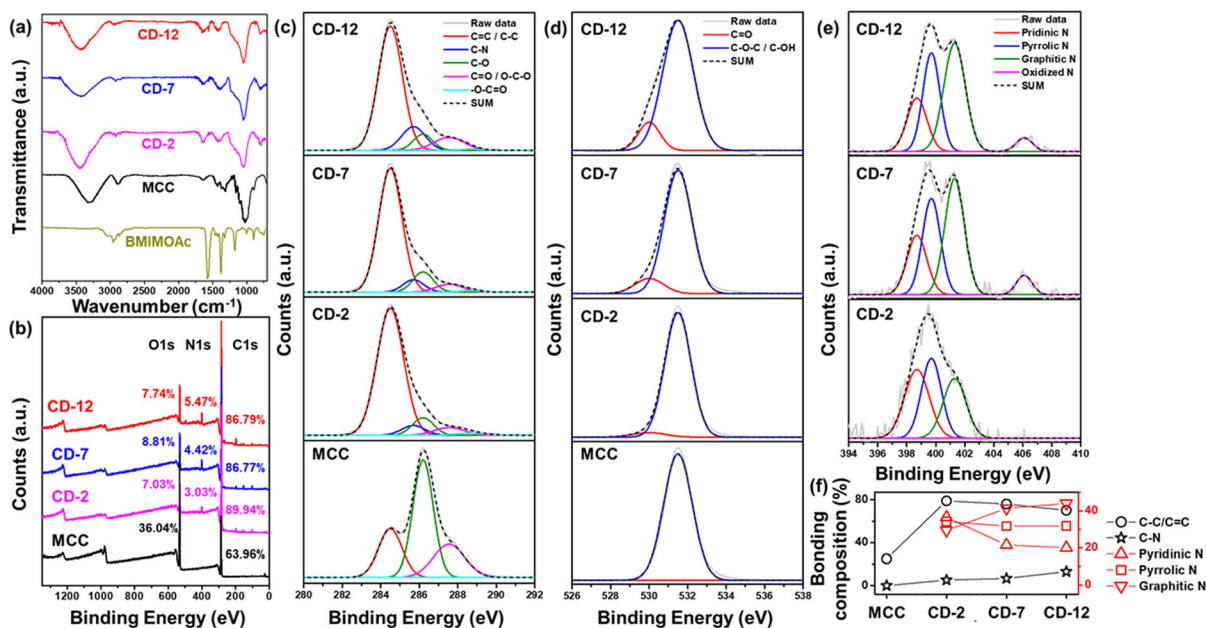

Fig. 2 **a** FT-IR spectra and **b** XPS survey spectra of BMIMOAc, MCC and carbon dots. High resolution XPS spectra of **c** C1s, **d** O1s, and **e** N1s and **f** bonding composition percent of MCC, CD-2, CD-7, and CD-12

2018; Jeong et al. 2018; Yang et al. 2014). The peak of ν(C–N) at 1560 cm^{-1} was intensified with the longer treatment time, confirming that nitrogen atom was successfully introduced and doped to the carbon dots (Ahn et al. 2017a; Zhai et al. 2012; Zhang et al. 2016).

To further characterize the chemical binding, the XPS spectra were obtained as shown in Fig. 2b. The XPS survey spectra of the carbon dots and MCC included C1s (284.5 eV) and O1s (531.5 eV) peaks. After the treatment, the calculated carbon contents of the specimens were increased from 64 to larger than 86%, while their oxygen contents were dramatically decreased from 36 to less than 8%. As coincident with the FT-IR results, it also indicates that the cellulose was successfully carbonized and converted to the carbon dots by the hydrolysis in IL. The high resolution C1s spectra (Fig. 2c) was deconvoluted to the peaks at 284.5 eV (C–C/C=C), 285.7 eV (C–N), 286.2 eV (C–O), 287.55 eV (C=O/O–C–O) and 288.7 eV (O–C=O) (Barsbay et al. 2007; Wu et al. 2017; Xie et al. 2018). Compared to MCC, the bonding composition percentage of C=C/C–C (284.5 eV) in the carbon dots was dramatically increased from 25 to 79%. As described above, the hydrolyzed molecules were condensed and polymerized into the graphitic core. With the longer treatment time, the sp^2 domains in the carbon dots were more developed by the self-generated acid in the cellulose/IL solutions (Jeong et al. 2018). Furthermore, the hydroxyl groups in the carbon dots were oxidized and converted to the carbonyl groups under acidic conditions, resulting in the bonding composition percentage of C=O peaks in O1s spectra increased from 4 to 13% (Fig. 2d). (Kang et al. 2012).

In the survey spectra, N1s peak (410 eV) was observed in the spectra of the carbon dots, which was not observed in the spectrum of MCC. The high-resolution N1s peaks of the carbon dots exhibit the four main peaks (Fig. 2e); pyridinic N (398.7 eV), pyrrolic N (399.7 eV), graphitic N (401.3 eV) and oxidized N (406.1 eV) (Ma et al. 2016; Shu et al. 2017). The calculated total content of the nitrogen in the carbon dots was increased from 3 to 5.5% along the treatment time. For the reaction time of 2 h, the binding states of the N atoms in the carbon dots were pyridinic N (36.4%), pyrrolic N (34.2%), and graphitic N (29.4%). As the treatment time increased up to 12 h, the graphitic N content in the carbon dots was dramatically increased from 29 to 44% (Fig. 2f).

Comparing to the graphitic N, the pyrrolic N, and pyridinic N were not changed significantly when the treatment time was increased from 7 to 12 h. As mentioned above, more acid was generated and in turn, accelerated the development of the graphitic core structure in longer treatment time (Ma et al. 2016; Ogi et al. 2016). Whereas, the oxidized N was found only in CD-7 and CD-12 not in CD-2, indicating that the nitrogen of the cyclic structure at the edge was oxidized by the acid (Pels et al. 1995; Shu et al. 2017). Based on the study of XPS, the change of the N state in the carbon dots can be summarized as follows. (1) Initially, the N-containing cyclic structures, i.e. pyrrolic N and pyridinic N were formed by IL. (2) These cyclic rings were developed to graphitic N in the core and simultaneously converted to oxidized N at the edge (Ma et al. 2016). The change in the chemical bonding of the carbon dots was summarized in Fig. 2f.

The optical properties of the carbon dots were characterized by UV–Vis and PL spectroscopy. The UV–Vis absorption of the carbon dots is shown in Fig. 3a. Two absorption peaks were observed at 253 and 310 nm, referring to π → π* transition of C=C and n → π* transition of C=O respectively (Edison et al. 2016; Shen et al. 2016; Wang et al. 2016; Wu et al. 2017). With the increase of treatment time, the absorption was increased in the total range of wavelength. Especially the shoulder peak at 310 nm was distinctly increased. It is attributed to the increase of n → π* transition in the carbonyl group of the carbon dots, which was increased along the treatment time (Ahn et al. 2019; He et al. 2017). As coincident to previous works, the increase of treatment time also raised the long-tailed absorption in high wavelength due to the increase of the functional groups on the surface such as carbonyl, amino groups (Tang et al. 2013; Yang et al. 2017).

Figure 3b displays the PL emission spectra of the carbon dots treated for different times. All PL emission of the carbon dots was depending on the excitation wavelength due to the variety of energy levels driven from the core structure and the functional groups (Arul et al. 2017; Tang et al. 2013). The PL emission intensities of the carbon dots were increased as the treatment time was increased. This PL enhancement was noticeable even by naked eyes as illustrated in the inserted images in the figure. Furthermore, the absolute quantum yields (QY) were 4.1, 20.2 and 28.4% for the treatment times of 2, 7 and 12 h,
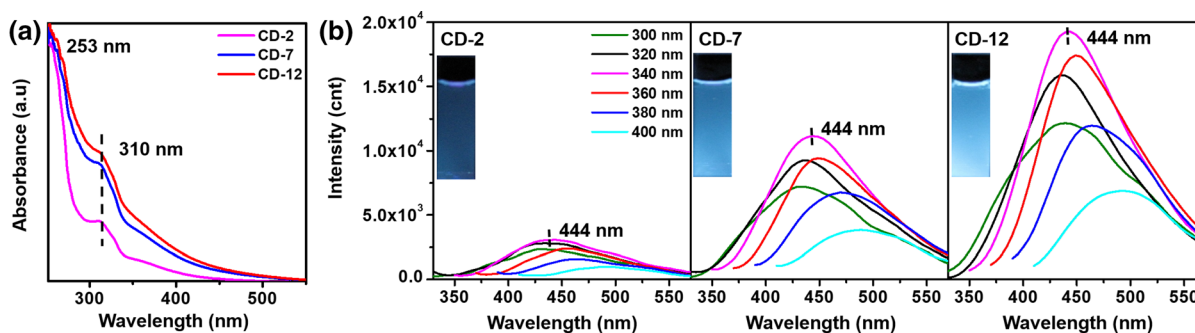
Fig. 3 a UV–Vis absorbance spectra and **b** PL emission spectra of the prepared carbon dots (inserted images: the aqueous solution of the carbon dots under 365 nm)

respectively. The dramatic increase of the QY was originated from the development of the graphitic structure and the nitrogen doping in the core. It gave more chances for the electron in the carbon dots to excite and recombine in radiative relaxation, resulting in the improvement of QY and PL emission (Ahn et al. 2019; Qu et al. 2014; Santiago et al. 2017).

Figure 4a shows the PL emissions images of CD-12 (50 μg/ml) in the absence and the presence of Fe^{3+} (250 μM) under 365 nm UV irradiation. The emission of CD-12 was noticeably quenched by Fe^{3+}. Within 15 min, the quenching was completed as shown in Fig. S1. To confirm the metal ion selectivity, the relative PL intensities of the solution with and without the competing metal ion were shown in Fig. 4b. The concentrations of the mixed metal salts and CD-12 were kept as 250 μM and 50 μg/ml, respectively. The changes of the PL intensity were characterized under the excitation of 340 nm which gave the maximum emission intensity. One is the intensity ratio of CD-12 solution between the presence and the absence of various metal ions (black bar in the figure), and the other is the intensity ratio of CD-12 in Fe^{3+} solution between the presence and the absence of each competing metal ion (red bar in the figure). As shown in the figure, the intensity was significantly decreased by Fe^{3+} even in the presence of the competing ion. The PL was selectively quenched by Fe^{3+} without the interference of other metal ions. The result reveals the excellent selective detectability of the prepared carbon dots against Fe^{3+}. Also, the carbon dots displayed good Fe^{3+} sensing ability even in tap water. In Fig. 4c, the fluorescence quenching efficiency $((F_0 - F)/F_0)$ was plotted along with the concentration of Fe^{3+}. The quenching efficiency was linearly increased as the

Fe^{3+} concentration increased from 2.5 to 37.5 μM, while the response was leveled off over the concentration of 37.5 μM. The fluorescence quenching mechanism of CD-12 in the linear relationship region against Fe^{3+} concentration was studied by the lifetime analysis. The PL decay curves of CD-12 were overlapped regardless of Fe^{3+} concentration (Fig. S2a). Moreover, the photoluminescence excitation (PLE) bands of CD-12 was mostly eclipsed with the absorption band of Fe^{3+} (Fig. S2b). This behavior was driven by the inner filter effect (Ahn et al. 2019; Yu et al. 2018; Zu et al. 2017). In the non-linear relationship region, CD-12 had more chance to form the complex with Fe^{3+}, resulting in the change of the absorption curves as shown in Fig. S2c (Shi et al. 2016; Wang et al. 2015; Zu et al. 2017). Using the Stern–Volmer equation, the fluorescence quenching efficiency in the linear range from 2.5 to 37.5 μM was regressed as shown in Fig. 4d. Based on the regression, the limit of detection (LOD) of CD-12 was calculated as 2.038 μM. Furthermore, CD-12 showed identical fluorescence quenching behavior even in the buffer solution as shown in Fig. S3.

The carbon dots in the study showed excellent PL stabilities under various conditions such as UV light, ionic strength, and pH change. The PL intensity was not significantly decreased after 9 months under daylight (Fig. S4a), while the PL intensity was slightly decreased after 4 h of UV exposure (Fig. S4b). However, the PL intensity of CD-12 remained as 80% of the initial intensity. Furthermore, the reduction of the PL intensity after UV exposure was simply recovered to the initial performance after 24 h storing in room condition (Fig. S4c). The effect of ionic strength on the PL intensity was evaluated in NaCl
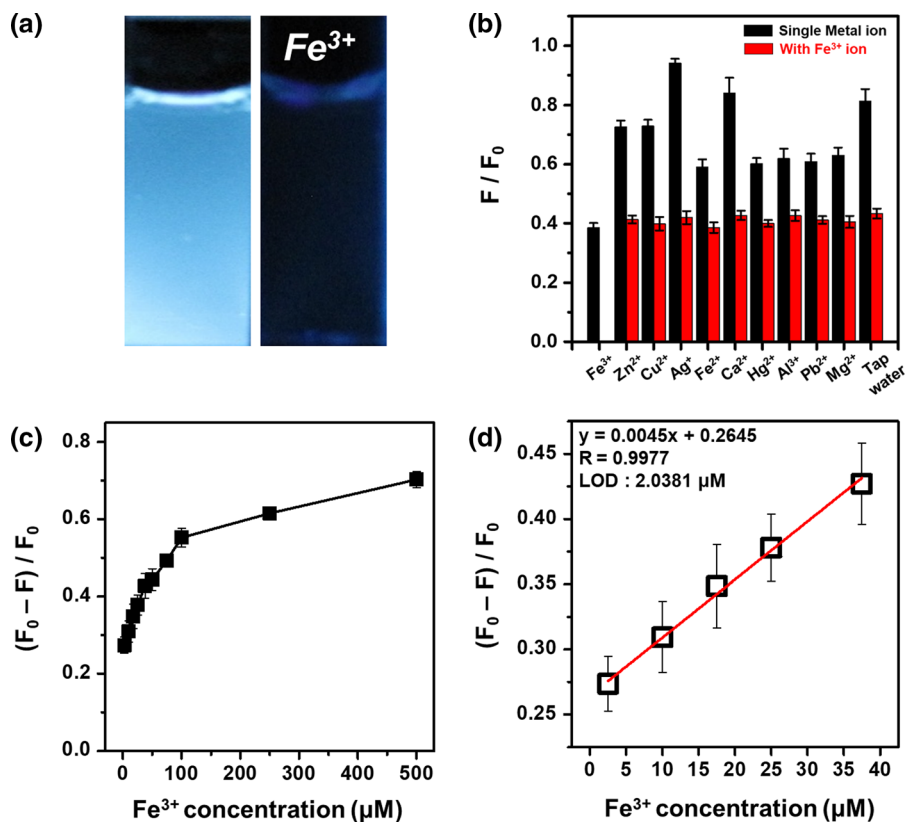
Fig. 4 **a** Digital images of CD-12 irradiated with UV light of 365 nm in the absence (left) and the presence of 250 μM Fe^{3+} (right)). **b** fluorescence quenching of CD-12 in different metal solutions (black) and mixed metal solutions with Fe^{3+} (red). **c** fluorescence quenching efficiency (($F_0 - F$)/F_0) of CD-12 versus the concentrations of Fe^{3+}. **d** Stern–Volmer plot of CD-12 in the Fe^{3+} concentration from 2.5 to 37.5 μM

solution. As shown in Fig. S5a, the PL intensities were not changed as the NaCl concentration was increased up to 1 M. It also indicates the prepared carbon dots in this work had high stability against the change of ionic strength in the aqueous solution. The PL behavior of CD-12 was characterized in different pH conditions (Fig. S5b). In general, the PL of carbon dots is reversibly changed by pH change due to the protonation and the deprotonation, when the carbon dots were not chemically reacted or damaged by acid or base (Feng et al. 2017; Liu and Zhou 2017; Shi et al. 2016). The carbon dots in this study showed the pH-dependent behavior along with the different pH conditions, and successfully recovered the PL intensity in neutral condition (Fig. S5c).

Figure 5 displays the optical properties of the CD-embedded cellulose film (CD-F). The film emitted blue light under UV light of 365 nm as shown in Fig. 5a. CD-F showed excellent transparency in

visible light range due to the good dispersion of the carbon dots and the amorphous structure of cellulose (Fig. S6 and Fig. S7a). The average transmittance at 400, 500, 600 and 700 nm was higher than 95%, which is higher than the reported values in other works (Table S1). Comparing with the pristine cellulose film, CD-F showed lower transmittance, especially in the UV range, as shown in Fig. S7b. It can be attributed to UV absorbance by the carbon dots in the UV range, which was confirmed by the transmittance difference between the pristine film and CD-F (Fig. S7c). The difference between the two spectra was obtained by subtracting the transmittance curve of CD-F from that of the pristine film. The transmittance difference curve was similar to the UV–Vis spectrum of CD-12 shown in Fig. 3a. As shown in Fig. S7d, the pristine film, and CD-F did not show a significant difference with the typical cellulose characteristic peaks (Ahn et al. 2017a, b). The peak at 1725 cm^{-1} of the CD-F was
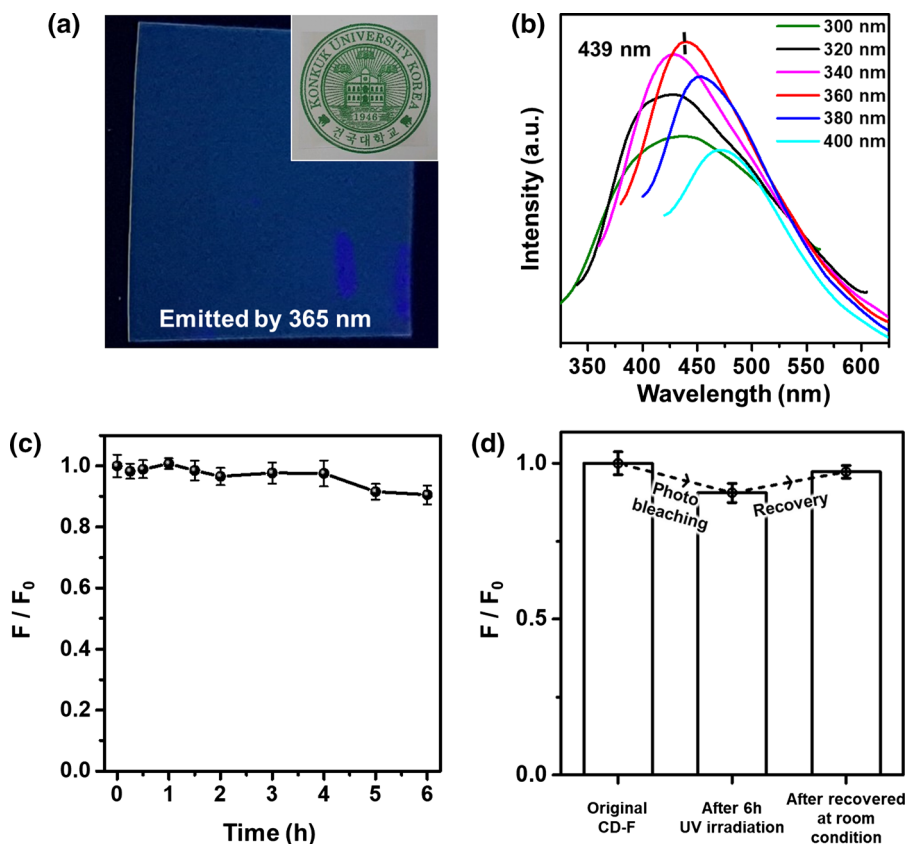
Fig. 5 **a** Digital images of CD-F under 365 nm (inserted image shows the transparency under daylight). **b** PL spectra of CD-F. **c** photostability of CD-F under UV irradiation (16 W, 365 nm). **d** PL recovery of CD-F after 24 h storing at room condition

driven from the carbon dots in the film. As similar to the carbon dots in aqueous solution, the CD-embedded film showed the dependency of the PL property on the excitation wavelength (Fig. 5b). The maximum PL intensity was observed around 440 nm under 360 nm excitation as like the carbon dots. It can also be attributed to the good dispersion of the carbon dots and the negligible formation of a non-radiative complex in the film. The photostability of CD-F was tested under UV irradiation (16 W, 365 nm). As shown in Fig. 5c., the PL intensity of CD-F remained as 90% of the initial intensity after 6 h of UV exposure. The PL intensity of CD-F was recovered by conditioning for 24 h (Fig. 5d).

The CD-embedded film can also detect Fe^{3+} efficiently as the carbon dots could (the inserted images in Fig. 6a). The PL emission of the film was quenched noticeably for naked eyes when the film was immersed for 30 s in a Fe^{3+} of 500 μM. Using the Stern–Volmer plot, the fluorescence quenching

efficiency along the Fe^{3+} concentration (2.5–500 μM) was obtained as illustrated in Fig. 6a. As similar to the carbon dots, the PL emission was quenched proportionally to the Fe^{3+} concentration in the low concentration region and was leveled off in the high concentration region.

Figure 6b shows the fluorescence quenching efficiency obtained from the regression of $(F_0 - F)/F_0$ along the Fe^{3+} concentration ranged from 2.5 to 17.5 μM. The film had a higher correlation coefficient (R = 0.9999) compared to the carbon dots, resulting in better LOD as 0.4077 μM. The quenching mechanism of the carbon dots in the film, as well as in the aqueous dispersion, showed the inner filter effect against Fe^{3+} ion (Fig. S8). As shown in Fig. 6c, the film quenched by Fe^{3+} can be recovered by simple washing for the repeated detection of Fe^{3+}. The maximum PL intensity was still observed around 440 nm under 360 nm excitation. By the repeats of the recovery, the PL intensity of the film was slightly decreased, while the
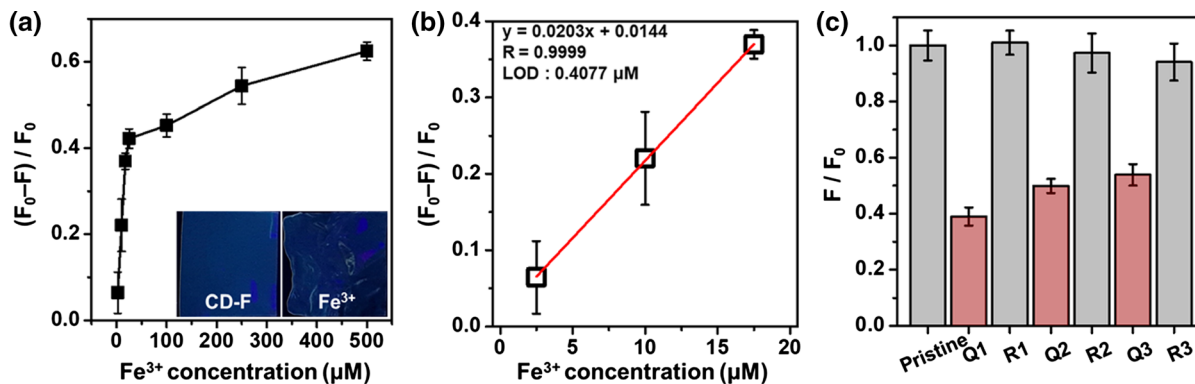
Fig. 6 a Fluorescence quenching efficiency $((F_0 - F)/F_0)$ of CD-F versus different concentrations of Fe^{3+} (inserted images: CD-F before (left) and after (right) immersion in 500 μM of Fe^{3+} under 365 nm). **b** Stern–Volmer plot of the CD-F in the Fe^{3+} concentration from 2.5 to 17.5 μM. **c** cycling test of the CD-F for Fe^{3+} sensing ('Q' refers to 'Quenching by Fe^{3+}' and 'R' refers to 'Recovery by washing')

relative PL intensity in the quenched state was increased. The result indicates that Fe^{3+} was combined with weak secondary bonding with the carbon dots in the film and could be removed by washing (Fang et al. 2018; Wu et al. 2017). The CD-embedded cellulose film can be repeatedly used for metal ion sensing with simple washing.

Conclusion

In this study, the carbon dots were fabricated from cellulose via solution synthesis using ionic liquid (IL). As the treatment time increased up to 12 h, the QY of the carbon dots was dramatically improved as 28.4% due to the development of the N-doped graphitic structure in the core and the functional groups on the surface. The carbon dots obtained after 12 h treatment showed good selective sensitivity toward Fe^{3+} with superior stability for long-term storage, UV exposure, ionic strength, and pH change. Using the CD-solution process, the CD-embedded cellulose film was successfully prepared via a one-pot process without additional separation for the carbon dots from the solution. The CD-embedded in the film had identical photoluminescent behavior to the carbon dots in the aqueous dispersion. As a Fe^{3+} indicating film, the CD-embedded cellulose film had the superior ability of simple reusability, selective sensitivity, and high photostability.

References

Abderrahim B et al (2015) Kinetic thermal degradation of cellulose, polybutylene succinate and a green composite: comparative study. World J Environ Eng 3:95

Ahn Y, Kwak S-Y, Song Y, Kim H (2016a) Physical state of cellulose in BmimCl: dependence of molar mass on viscoelasticity and sol-gel transition. Phys Chem Chem Phys 18:1460–1469

Ahn Y, Song Y, Kwak S-Y, Kim H (2016b) Highly ordered cellulose II crystalline regenerated from cellulose hydrolyzed by 1-butyl-3-methylimidazolium chloride. Carbohydr Polym 137:321–327

Ahn Y, Song Y, Kim H (2017a) In situ formation of autodispersing cellulose nanoparticles with extreme uniformity. ACS Macro Lett 6:762–767

Ahn Y, Song Y, Kim H, Kwak S-Y (2017b) Formation of cellulose-carbene complex via depolymerization in ILs: dependence of IL types on kinetics, conformation and dispersity. Carbohydr Polym 159:86–93

Ahn J et al (2019) Food waste-driven N-doped carbon dots: applications for Fe^{3+} sensing and cell imaging. Mater Sci Eng C 102:106–112

Arul V, Edison TNJI, Lee YR, Sethuraman MG (2017) Biological and catalytic applications of green synthesized fluorescent N-doped carbon dots using *Hylocereus undatus*. J Photochem Photobiol B Biol 168:142–148

Barsbay M et al (2007) Verification of controlled grafting of styrene from cellulose via radiation-induced RAFT polymerization. Macromolecules 40:7140–7147

Börjesson M, Westman G (2015) Crystalline nanocellulose-preparation, modification, and properties. In: Poletto M, Ornaghi H Jr (eds) Cellulose-fundamental aspects and current trends. IntechOpen, London, pp 159–191

Chae A et al (2018) Mechanochemical synthesis of fluorescent carbon dots from cellulose powders. Nanotechnology 29:165604

Coates J (2000) Interpretation of infrared spectra, a practical approach. In: Meters RA (ed) Encyclopedia of analytical chemistry. Wiley, Chichester, pp 10815–10837

da Silva Souza DR, Caminhas LD, de Mesquita JP, Pereira FV (2018) Luminescent carbon dots obtained from cellulose. Mater Chem Phys 203:148–155

Du H, Qian X (2011) The effects of acetate anion on cellulose dissolution and reaction in imidazolium ionic liquids. Carbohydr Res 346:1985–1990

Edison TNJI et al (2016) Microwave assisted green synthesis of fluorescent N-doped carbon dots: cytotoxicity and bio-imaging applications. J Photochem Photobiol B Biol 161:154–161

Fang B-Y et al (2018) Nitrogen-doped graphene quantum dot for direct fluorescence detection of Al^{3+} in aqueous media and living cells. Biosens Bioelectron 100:41–48

Feng Z et al (2017) Nitrogen-doped carbon quantum dots as fluorescent probes for sensitive and selective detection of nitrite. Molecules 22:2061

Gu D, Shang S, Yu Q, Shen J (2016) Green synthesis of nitrogen-doped carbon dots from lotus root for Hg(II) ions detection and cell imaging. Appl Surf Sci 390:38–42

Gu J et al (2018) Green synthesis of amphiphilic carbon dots from organic solvents: application in fluorescent polymer composites and bio-imaging. RSC Adv 8:12556–12561

Guo Y, Zhang L, Cao F, Leng Y (2016) Thermal treatment of hair for the synthesis of sustainable carbon quantum dots and the applications for sensing Hg^{2+}. Sci Rep 6:35795

He G et al (2017) Microwave formation and photoluminescence mechanisms of multi-states nitrogen doped carbon dots. Appl Surf Sci 422:257–265

Huddleston JG et al (2001) Characterization and comparison of hydrophilic and hydrophobic room temperature ionic liquids incorporating the imidazolium cation. Green Chem 3:156–164

Ishida H et al (2010) Recent advances in instrumentation for absolute emission quantum yield measurements. Coord Chem Rev 254:2449–2458

Jeong Y et al (2018) Converting waste papers to fluorescent carbon dots in the recycling process without loss of ionic liquids and bioimaging applications. ACS Sustain Chem Eng 6:4510–4515

Kang S, Li X, Fan J, Chang J (2012) Characterization of hydrochars produced by hydrothermal carbonization of lignin, cellulose, D-xylose, and wood meal. Ind Eng Chem Res 51:9023–9031

Kim H, Ahn Y, Kwak S-Y (2016) Comparing the influence of acetate and chloride anions on the structure of ionic liquid pretreated lignocellulosic biomass. Biomass Bioenergy 93:243–253

Kim Y, Song Y, Kim H (2018) Preparation of transparent cellulose film with controlled haze using halloysite nanotubes. Cellulose 25:1239–1248

Lee SH, Doherty TV, Linhardt RJ, Dordick JS (2009) Ionic liquid- mediated selective extraction of lignin from wood leading to enhanced enzymatic cellulose hydrolysis. Biotechnol Bioeng 102:1368–1376

Liu Y, Zhou Q (2017) Sensitive pH probe developed with water-soluble fluorescent carbon dots from chocolate by one-step hydrothermal method. Int J Environ Anal Chem 97:1119–1131

Liu S et al (2011) Preparation of photoluminescent carbon nitride dots from CCl4 and 1, 2-ethylenediamine: a heat-treatment-based strategy. J Mater Chem 21:11726–11729

Liu R et al (2015) An ionic liquid promoted microwave-hydrothermal route towards highly photoluminescent carbon dots for sensitive and selective detection of iron (III). RSC Adv 5:24205–24209

Loi E et al (2017) One- pot synthesis of carbon dots using two different acids and their respective unique photoluminescence property. Luminescence 32:114–118

Lu J et al (2009) One-pot synthesis of fluorescent carbon nanoribbons, nanoparticles, and graphene by the exfoliation of graphite in ionic liquids. ACS Nano 3:2367–2375

Ma R et al (2016) Ionic liquid-assisted synthesis of dual-doped graphene as efficient electrocatalysts for oxygen reduction. Carbon 102:58–65

MináKim S et al (2015) In situ synthesis of luminescent carbon nanoparticles toward target bioimaging. Nanoscale 7:5468–5475

Ng YH, Chin SF, Pang SC, Ng SM (2017) The luminescence profile of carbon dots synthesized from α-cellulose under different acid hydrolysis conditions. Opt Mater 70:50–56

Nie H et al (2014) Carbon dots with continuously tunable full-color emission and their application in ratiometric pH sensing. Chem Mater 26:3104–3112

Ogi T et al (2016) Kinetics of nitrogen-doped carbon dot formation via hydrothermal synthesis. New J Chem 40:5555–5561

Ou R et al (2012) Solid biopolymer electrolytes based on all-cellulose composites prepared by partially dissolving cellulosic fibers in the ionic liquid 1-butyl-3-methylimidazolium chloride. J Mater Sci 47:5978–5986

Pels J et al (1995) Evolution of nitrogen functionalities in carbonaceous materials during pyrolysis. Carbon 33:1641–1653

Qu D et al (2014) Formation mechanism and optimization of highly luminescent N-doped graphene quantum dots. Sci Rep 4:5294

Ren J et al (2019) Influence of surface chemistry on optical, chemical and electronic properties of blue luminescent carbon dots. Nanoscale 11:2056–2064

Santiago S et al (2017) Synthesis of N-doped graphene quantum dots by pulsed laser ablation with diethylenetriamine (DETA) and their photoluminescence. Phys Chem Chem Phys 19:22395–22400

Sevilla M, Fuertes AB (2009) The production of carbon materials by hydrothermal carbonization of cellulose. Carbon 47:2281–2289

Shen P, Gao J, Cong J, Liu Z, Li C, Yao J (2016) Synthesis of cellulose- based carbon dots for bioimaging. ChemistrySelect 1:1314–1317

Shi L et al (2016) Controllable synthesis of green and blue fluorescent carbon nanodots for pH and Cu^{2+} sensing in living cells. Biosens Bioelectron 77:598–602

Shu Y et al (2017) Ionic liquid mediated organophilic carbon dots for drug delivery and bioimaging. Carbon 114:324–333

Silva SS, Mano JF, Reis RL (2017) Ionic liquids in the processing and chemical modification of chitin and chitosan for biomedical applications. Green Chem 19:1208–1220

Song Y et al (2017) Morphological and chemical structure of hydrothermally carbonized saccharides. Fiber Polym 18:1602–1608

Su H, Bi Z, Ni Y, Yan L (2019) One-pot degradation of cellulose into carbon dots and organic acids in its homogeneous aqueous solution. Green Energy Environ 4:391–399

Tan X, Li X, Chen L, Xie F (2016) Solubility of starch and microcrystalline cellulose in 1-ethyl-3-methylimidazolium acetate ionic liquid and solution rheological properties. Phys Chem Chem Phys 18:27584–27593

Tang L et al (2013) Energy-level structure of nitrogen-doped graphene quantum dots. J Mater Chem C 1:4908–4915

Trache D, Hussin MH, Haafiz MM, Thakur VK (2017) Recent progress in cellulose nanocrystals: sources and production. Nanoscale 9:1763–1786

Wang Y et al (2014) Lignin dissolution in dialkylimidazolium-based ionic liquid–water mixtures. Bioresour Technol 170:499–505

Wang S, Chen Z-G, Cole I, Li Q (2015) Structural evolution of graphene quantum dots during thermal decomposition of citric acid and the corresponding photoluminescence. Carbon 82:304–313

Wang C et al (2016) Synthesis of cellulose-derived carbon dots using acidic ionic liquid as a catalyst and its application for detection of Hg^{2+}. J Mater Sci 51:861–867

Wei L, Li K, Ma Y, Hou X (2012) Dissolving lignocellulosic biomass in a 1-butyl-3-methylimidazolium chloride–water mixture. Ind Crop Prod 37:227–234

Wu R-L et al (2009) Green composite films prepared from cellulose, starch and lignin in room-temperature ionic liquid. Bioresour Technol 100:2569–2574

Wu P et al (2017) Hydrothermal synthesis of nitrogen-doped carbon quantum dots from microcrystalline cellulose for the detection of Fe^{3+} ions in an acidic environment. RSC Adv 7:44144–44153

Xiao D et al (2016) One-step hydrothermal synthesis of photoluminescent carbon nitride dots derived from ionic liquids. New J Chem 40:320–324

Xie Y et al (2018) Surface hydrophobic modification of microcrystalline cellulose by poly (methylhydro) siloxane using response surface methodology. Polymers 10:1335

Xu M et al (2013) Hydrothermal/solvothermal synthesis of graphene quantum dots and their biological applications. Nano Biomed Eng 5:65–71

Yang X et al (2014) Novel and green synthesis of high-fluorescent carbon dots originated from honey for sensing and imaging. Biosens Bioelectron 60:292–298

Yang G et al (2016) Acidophilic S-doped carbon quantum dots derived from cellulose fibers and their fluorescence sensing performance for metal ions in an extremely strong acid environment. J Mater Chem A 4:12841–12849

Yang J et al (2017) Hydrothermal synthesis and photoluminescent mechanistic investigation of highly fluorescent nitrogen doped carbon dots from amino acids. Mater Res Bull 89:26–32

Yesudass S et al (2016) Experimental and theoretical studies on some selected ionic liquids with different cations/anions as corrosion inhibitors for mild steel in acidic medium. J Taiwan Inst Chem E 64:252–268

Yu J et al (2018) Luminescence mechanism of carbon dots by tailoring functional groups for sensing Fe^{3+} ions. Nanomaterials 8:233–244

Zhai X et al (2012) Highly luminescent carbon nanodots by microwave-assisted pyrolysis. Chem Commun 48:7955–7957

Zhang P et al (2014) Updating biomass into functional carbon material in ionothermal manner. ACS Appl Mater Interfaces 6:12515–12522

Zhang B et al (2015) Understanding the structural disorganization of starch in water–ionic liquid solutions. Phys Chem Chem Phys 17:13860–13871

Zhang Y et al (2016) Effect of reaction temperature on structure and fluorescence properties of nitrogen-doped carbon dots. Appl Surf Sci 387:1236–1246

Zheng B et al (2015) One pot selective synthesis of water and organic soluble carbon dots with green fluorescence emission. RSC Adv 5:11667–11675

Zu F et al (2017) The quenching of the fluorescence of carbon dots: a review on mechanisms and applications. Microchim Acta 184:1899–1914